ACS OMEGA

http://pubs.acs.org/journal/acsodf

Article

Influence of Hydroxyl Groups on the Inhibitive Corrosion of Gemini Surfactant for Carbon Steel

Chengxian Yin,* Minjian Kong, Juantao Zhang, Yuan Wang, Qingwei Ma, Qibin Chen,* and Honglai Liu

Cite This: *ACS Omega* 2020, 5, 2620−2629

Read Online

ACCESS | Metrics & More | Article Recommendations | Supporting Information

ABSTRACT: The corrosion inhibition performance of propanediyl-1,3-bis(*N*,*N*-dimethyl-*N*-dodecylammonium bromide) and propanediyl-1,3-bis(*N*,*N*-dihydroxyethyl-*N*-dodecylammonium bromide), abbreviated as PDDB and PDHDB, respectively, for carbon steel in 1.0 mol·L^{-1} hydrochloric acid solution was investigated using the gravimetric method and various electrochemical techniques, together with scanning electron microscopy and energy-dispersive spectrometry. Results show that PDHDB always has a better inhibition performance relative to PDDB, which can be attributed to the introduction of hydroxyl groups at the hydrophilic headgroups, thereby causing an extra interaction between inhibitors and the metal surface and favoring its adsorption. These findings highlight that the modification to the headgroups of Gemini-type inhibitors may be another effective approach to improving their inhibition performance.

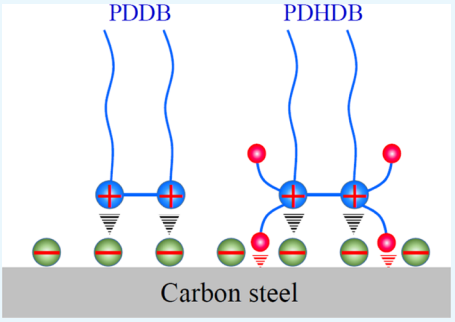

1. INTRODUCTION

Carbon steel is very often applied in diverse industrial fields, including building; chemical processing; oil/gas storage and transportation; process vessel, equipment, and pipeline; and so forth, due to its low cost, incredible mechanical workability, and easy availability for constructing various vessels.[1,2] Nevertheless, any environment containing water has a notable potential to generate corrosive activity, since it can inevitably dissolve gases (e.g., O_2 and CO_2) and mineral salts. For instance, in petroleum and natural gas industries, oil field formation water always contains high-concentration chlorides, carbonates, sulfates, and dissolved gases, such as H_2S and CO_2, thereby causing massive economic loss. Also, in many industrial processes, acid solutions are widely used for cleaning, pickling, descaling, etching of metal, and oil well acidizing. Unfortunately, carbon steel is dramatically sensitive to being corroded in contact with various aggressive media, especially in the acidic environment.[3] To address acid corrosion, the use of inhibitors is one of the most effective and practical methods to prevent carbon steel from the corrosion and reduce the corrosive attack. In principle, inhibitors normally function by adsorbing on the metal surface and then forming a compact barrier layer, thereby protecting the metal against corrosion; moreover, the adsorption interactions can generally be classified into two categories: physisorption via electrostatic interactions and chemisorption via the formation of coordinate covalent bonds.[3] Among various inhibitors, Gemini surfactants are considered to be a promising candidate in the anticorrosion applications due to their unique molecular structures and outstanding surface properties.[4,5] To date, bis(quaternary ammonium)-type Gemini surfactants have widely been investigated in anticorrosion applications as inhibitors.[4]

As effective inhibitors, the used organic compounds are generally required to contain heteroatoms bearing lone-pair electrons, such as S, P, O, N, etc., multiple (double and/or triple) bonds, and conjugated aromatic circles, since the chemisorption, having a stronger interaction relative to physisorption, can be facilitated by the charge sharing or transfer from such electron-rich functional groups to the metal surface.[6,7] Accordingly, various heteroatoms or aromatic rings should be introduced into one of three moieties (structural variables) in such bis(quaternary ammonium) Gemini surfactants, i.e., the spacer, hydrophobic tail, and hydrophilic head, due to the possibility of forming coordinate bonds, to improve their adsorption effectiveness and inhibition efficiencies (IEs).[8−15] However, the current interest has so far concentrated mainly on modifying the spacer of Gemini-type inhibitors by means of using heteroatoms or double/triple bonds, with the exception of using the hydroxyethyl to replace the methyl at the quaternary ammonium headgroups.[10] Moreover, among such inhibitors, the quaternary ammonium salt was commonly chosen as the headgroup. In essence, the high-efficiency inhibition action is thought to originate from the tightly packed layer of inhibitors that can cover the metal

Received: September 13, 2019
Accepted: January 13, 2020
Published: February 4, 2020

https://dx.doi.org/10.1021/acsomega.9b02989
ACS Omega 2020, 5, 2620−2629

surface and isolate the metal from the aggressive medium.[16−19] In spite of its popularity, many fundamental questions surrounding the adsorption of Gemini inhibitors remain to be answered.[4,20] Particularly, the role and the size of heteroatom-containing substitutes have not been firmly established yet.[4,10] Therefore, in the present work, our primary objective of introducing an electronegative heteroatom into the headgroups in such bis(quaternary ammonium) Gemini inhibitors was twofold: (i) to assess its influence on the inhibition performances and (ii) to judge the role that the modified functional groups play.

To address these issues, a new cationic Gemini-type surfactant, propanediyl-1,3-bis(*N*,*N*-dihydroxyethyl-*N*-dodecylammonium bromide), abbreviated as PDHDB (Chart 1), was synthesized as an inhibitor. To shed more light on the inhibitory action, an analogous counterpart, propanediyl-1,3-bis(dimethyldodecyl-ammonium bromide), referred to as PDDB (Chart 1), was also included in this work. The inhibition performances of both surfactants were investigated and compared carefully by means of the gravimetric method, potentiodynamic polarization (PDP) measurement, and electrochemical impedance spectroscopy (EIS) technique. Results show that the introduction of hydroxyl groups into the headgroups does favor enhancing the IE value. Our findings highlight the need for taking a wide range of the combination of structural variables in inhibitors into consideration when designing their molecular structures and optimizing their inhibition properties.

Chart 1. Chemical Structures of PDDB and PDHDB

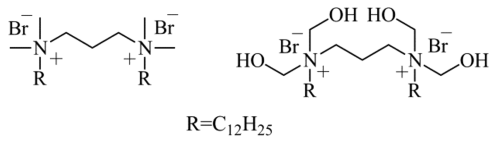

PDDB PDHDB

2. RESULTS AND DISCUSSION

2.1. Gravimetric Measurements. The gravimetric measurement is a reliable method to judge the effect of the concentration of inhibitors on IEs. All results obtained from gravimetric measurements in the HCl solution without inhibitors and with PDDB or PDHDB at different concentrations, including IEs, corrosion rate, and surface coverage, are compiled in Table 1. Herein, the corrosion rate (v in millimeters per year, mm·y^{-1}) of carbon steel in the absence and presence of PDDB or PDHDB with different concentrations was determined in terms of the mass loss values after 6 h immersion at 25.0 °C,[21] which was calculated via eq 1 as follows

$$v = \frac{K \times \Delta m}{\rho \times S \times t} \quad (1)$$

where K is a constant (8.76×10^4); Δm (g) and ρ (g·cm^{-3}) are the mass loss of carbon steel specimens and the carbon steel density (7.86 g·cm^{-3}), respectively; and S (cm^2) and t (h) are the exposed surface area and the immersion time, respectively.

On the basis of the calculated corrosion rates, the IE (η) values were calculated according to eq 2

$$\eta = \frac{v_0 - v}{v_0} \times 100\% \quad (2)$$

where v_0 (mm·y^{-1}) and v (mm·y^{-1}) are the corrosion rates of carbon steel coupons in a 1.0 mol·L^{-1} HCl solution in the absence and presence of inhibitors, respectively.

Since the inhibitory corrosion action was based on adsorption, in which most of the electroactive sites had been effectively blocked by adsorbed inhibitors, the corrosion rate could be considered as a measure of the number of free corrosion sites remaining. If assuming that the corrosion only took place at such free sites and the blocked site had a negligible contribution to the total corrosion rate, the IE values were thus correlated with the surface coverage (θ) directly.[22] Accordingly, a widely used relation between θ and η had been proposed, given in eq 3[23]

$$\theta = \frac{\eta\ (\%)}{100} \quad (3)$$

Figure 1 shows the variation profiles of IEs, coupled with corrosion rates, with the logarithmic concentration (C) of PDDB and PDHDB. Obviously, in the range of lower concentrations of inhibitors, the IE values increase sharply with increasing concentrations, whereas these values gradually level off as the concentrations are raised. By comparison, the change in the corrosion rates shows an opposite tendency: initially decreasing rapidly, then leveling off. That is to say, the IE value increases with the incremental concentrations of inhibitors, while the corrosion rate decreases. These changes in IEs and corrosion rates can be ascribed to the adsorption of PDHDB and PDDB, where the adsorption amount increases with increasing concentrations of inhibitors, thereby forming a

Table 1. Corrosion Parameters of PDDB and PDHDB Obtained from Weight Loss Measurements for Carbon Steel in 1.0 mol·L^{-1} HCl

inhibitor	C/mol·L^{-1}	v/mm·y^{-1}	θ	η (%)
HCl	0	4.9945 ± 0.1258		
PDDB	1.0×10^{-6}	2.9201 ± 0.0119	0.42 ± 0.01	41.6 ± 0.2
	3.0×10^{-6}	1.7116 ± 0.0501	0.66 ± 0.01	65.7 ± 1.0
	6.0×10^{-6}	1.6018 ± 0.0066	0.68 ± 0.01	67.9 ± 0.2
	1.0×10^{-5}	1.0839 ± 0.1095	0.78 ± 0.02	78.4 ± 2.4
	3.0×10^{-5}	0.6813 ± 0.0573	0.86 ± 0.02	86.3 ± 1.2
PDHDB	1.0×10^{-6}	2.5153 ± 0.0692	0.49 ± 0.01	49.4 ± 1.2
	3.0×10^{-6}	1.6220 ± 0.0459	0.68 ± 0.01	67.5 ± 0.9
	6.0×10^{-6}	1.3084 ± 0.1115	0.75 ± 0.01	74.5 ± 1.5
	1.0×10^{-5}	0.8670 ± 0.0678	0.83 ± 0.02	82.7 ± 1.4
	3.0×10^{-5}	0.5742 ± 0.0686	0.89 ± 0.02	88.5 ± 1.3

https://dx.doi.org/10.1021/acsomega.9b02989
ACS Omega 2020, 5, 2620−2629

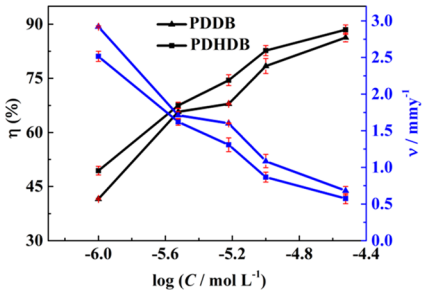

Figure 1. Variations of IEs and corrosion rates of carbon steel with the logarithmic concentrations of PDDB and PDHDB in 1.0 mol·L^{-1} HCl.

protective film of inhibitor adsorbed and retarding the corrosion.

In the present work, both PDHDB and PDDB present a good inhibitive performance in relatively low-concentration ranges, even when the concentration was as low as 1.0×10^{-5} mol·L^{-1}. More importantly, as expected, in the entire concentration range, PDHDB shows better inhibitive performance than PDDB. This can be attributed to the introduction of the hydroxyls at the headgroups in the former case, thereby causing a strong interaction between inhibitors and the metal surface, which can be further confirmed by the following characterizations and analyses.

2.2. Adsorption Isotherms. The adsorption of inhibitor molecules at the metal surface/solution interface can routinely provide information about their interactions with the metal surface and interactions among the adsorbed inhibitors themselves as well. Since the adsorption of inhibitors is of a quasi-equilibrium nature, an appropriate adsorption isotherm can be allowed to represent this procedure. In the present study, the surface coverage values were obtained from the gravimetric data and the Langmuir adsorption isotherm model was used to fit these experimental data of PDDB and PDHDB, affording high regression coefficients of R^2 = 0.99888 and 0.99970, respectively, and slope values slightly larger than unity (1.116 and 1.086 for PDDB and PDHDB, respectively), as given in Figure 2 and Table 2. The former suggests that the

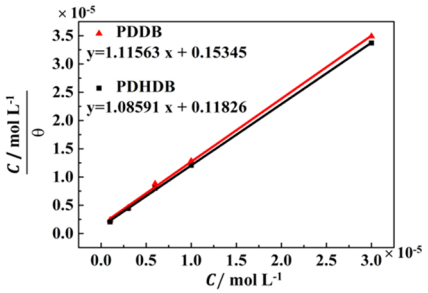

Figure 2. Langmuir adsorption isotherms of PDDB or PDHDB on the surface of carbon steel in 1 mol·L^{-1} HCl.

Table 2. Thermodynamic Parameters of PDDB and PDHDB Adsorbed on Carbon Steel in 1 mol·L^{-1} HCl

inhibitor	K_{ads}/×10^3 L·mol^{-1}	ΔG_{ads}/kJ·mol^{-1}	R^2
PDDB	651.68	−43.14	0.99888
PDHDB	845.59	−43.79	0.99970

experimental data are well described by the Langmuir adsorption isotherm, that is, the adsorption process of PDDB or PDHDB conforms to the Langmuir isothermal adsorption. The latter denotes that such a deviation in the slope from unity is a likely consequence of the presence of an intermolecular weak interaction among the adjacent adsorbed molecules, since this interaction is theoretically ignored during deriving the Langmuir adsorption isotherm.[24,25]

In the Langmuir model, the surface coverage, θ, can be correlated with the inhibitor concentration, C, in terms of eq 4[26]

$$\frac{C}{\theta} = \frac{1}{K_{ads}} + C \tag{4}$$

where K_{ads} denotes the adsorption equilibrium constant in the adsorption process. Herein, K_{ads}, obtained from the intercept of the Langmuir isotherm, displays much higher values, given in Table 2, meaning that PDDB and PDHDB can preferentially adsorb on the carbon steel surface and thus deliver great IE values.

The equilibrium constant, K_{ads}, could be applied to determine the standard Gibbs free energy of the adsorption process, ΔG_{ads}, by means of eq 5[27]

$$\Delta G_{ads} = -RT \ln(55.5 \times K_{ads}) \tag{5}$$

where the value 55.5 (mol·L^{-1}) represents the molar concentration of water in solution, R (J·mol^{-1}·K^{-1}) is the universal gas constant gas of 8.314, and T (K) is the absolute temperature. In this work, the ΔG_{ads} values of PDDB and PDHDB were calculated to be −43.14 and 43.79 kJ·mol^{-1}, respectively, which are also given in Table 2.

The negative values of ΔG_{ads} demonstrate that their adsorption is a spontaneous process and both of them can adsorb on the carbon steel surface and form a defensive film. In general, when the physisorption process takes place, the corresponding ΔG_{ads} values are usually close to or less than −20 kJ·mol^{-1} in virtue of the electrostatic interaction; in contrast, if the chemisorption process occurs, ΔG_{ads} displays a more negative value, i.e., close to or higher than −40 kJ·mol^{-1}, due to the formation of a coordinate covalent bond.[6,23,28] Herein, PDHDB and PDDB present more negative values, i.e., −43.79 and −43.14 kJ·mol^{-1}, respectively, which are in a good agreement with those of analogues reported recently.[22,29] In these two studies, Gao et al. and Mobin et al. attributed the more negative ΔG_{ads} values (less than −40 kJ·mol^{-1}) to cationic Gemini-type inhibitors having the special molecular structure, hence endowing themselves with a high adsorption ability and in turn forming a strong protective film.[22,29] However, as discussed elsewhere,[17,30−32] the adsorption of inhibitors on metal surfaces cannot only be considered to be pure physisorption or chemisorption. Except for the chemisorption (if it does), inhibitors can also be adsorbed on the metal surfaces by means of physical interactions. As a result, in the present work, it is concluded that: (i) considering the fact that a PDDB molecule can dissociate into only one bivalent cation and two Br$^-$ anions, the adsorption of PDDB molecules on the carbon steel surface is an integrated type of physical and chemical adsorptions, but with a predominant electrostatic interaction (physisorption), and (ii) on the basis of the difference in the molecular structures and the IEs between PDDB and PDHDB, the presence of hydroxyethyl groups in PDHDB can contribute to the chemisorption to some extent.

https://dx.doi.org/10.1021/acsomega.9b02989
ACS Omega 2020, 5, 2620−2629

2.3. Open-Circuit Potential (OCP) versus Immersion Time. Figure 3 shows the variation of the open-circuit potential (E_{OCP}) of working electrodes versus the Ag/AgCl electrode as a function of immersion time in the aerated and unstirred 1.0 mol·L^{-1} HCl solution in the absence and presence of PDDB or PDHDB with a concentration of 3.0 × 10^{-5} mol·L^{-1}. Herein, the E_{OCP} value in the blank HCl solution anodically shifted to more positive potentials and then gradually leveled off after an immersion time of 1500 s. This can be attributed to the initial dissolution process of the air-formed oxide layer at the carbon steel surface and the attack on the bare metal as well. By contrast, the addition of PDDB or PDHDB led to the fact that the steady potentials were attained more readily; moreover, the steady state presented a slight positive (PDDB) and negative (PDHDB) shift in E_{OCP}, which is a likely result of forming a protective film on the metal surface and thus impeding the anodic or cathodic sites.[33,34] However, the maximum shift in E_{OCP} was less than 20 mV after adding PDDB or PDHDB, denoting that both of them behave as mixed-type inhibitors.

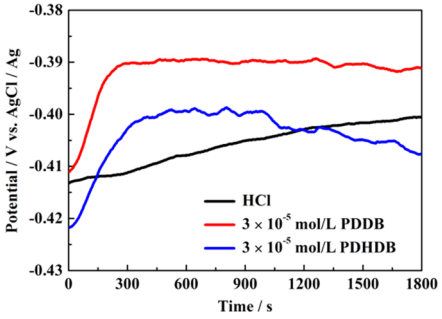

Figure 3. Variation of potentials with immersion time for carbon steel in 1.0 mol·L^{-1} HCl solution in the absence and presence of 3 × 10^{-5} mol·L^{-1} PDDB and PDHDB.

2.4. Potentiodynamic Polarization (PDP) Measurements. Figure 4 shows the PDP curves for the carbon steel in 1.0 mol·L^{-1} HCl solution without and with the addition of various concentrations (from 1.0 × 10^{-6} to 3.0 × 10^{-5} mol·L^{-1}) of PDDB (A) and PDHDB (B). To shed more light on the kinetics process of the carbon steel dissolution, the related electrochemical parameters, such as corrosion potential (E_{corr}), corrosion current density (I_{corr}), anodic (β_a) and cathodic (β_c) Tafel slopes, and IEs (η), were determined and are compiled in Table 3. The η values of PDDB and PDHDB were calculated using eq 6

$$\eta = \frac{I_{corr} - I_{inh}}{I_{corr}} \times 100\% \quad (6)$$

where I_{corr} and I_{inh} are the corrosion current densities in mA·cm^{-2} before and after adding inhibitors, respectively, derived from extrapolating the cathodic and anodic Tafel lines to the corrosion potential.

As is apparent, a concentration-dependent shift in both the anodic and cathodic branches toward lower values of current density was observed; moreover, the higher the concentration, the more prominent the shift becomes. That is to say, the addition of PDDB and PDHDB leads to a dramatic reduction in the I_{corr} values: the I_{corr} values shift from 0.2081 mA·cm^{-2} (blank) to 0.0235 mA·cm^{-2} for PDDB and to 0.0233 mA·cm^{-2} for PDHDB, at the concentration of 3.0 × 10^{-5} mol·L^{-1}. This means that in aggressive media, both cathodic hydrogen evolution and anodic dissolution reactions are dramatically inhibited with the increase in concentrations. In Table 3, both the β_c and β_a values present only a slight variation, indicating that PDDB and PDHDB both function by blocking the contact of HCl with the metal surface due to their adsorption but do not significantly alter the mechanism of the corrosion reaction.[30] Furthermore, there is no definite trend in the shift of the corrosion potential (E_{corr}) in the presence of PDDB and PDHDB with their increasing concentrations, and the absolute value of the maximum shift in ΔE_{corr} is nearly less than 15 mV, suggesting that the inhibition action may stem from the geometric blocking effect.[33] Taken together, the reduction in anodic and cathodic current densities and the slight variation in β_c and β_a slopes denote that both PDDB and PDHDB, together with the shift in E_{corr}, behave as mixed-type inhibitors, consistent with the OCP result, and act on both the cathodic hydrogen evolution reaction and the anodic metal dissolution reaction,[35−37] thereby yielding an increase in the IE values. In addition, it is noteworthy that the variation of IEs with the concentration obtained from gravimetric and PDP measurements presents a good agreement; moreover, the IE value of PDHDB is always better than that of PDDB in the entire concentration range.

In this work, the IEs nearly reach separately up to 89% for PDDB and PDHDB, based on PDP data, suggesting that both inhibitors have a good inhibition action, especially in their low- and moderate-concentration ranges. To address this issue, an IE comparison between our inhibitors (PDDB and PDHDB) and analogous bis(quaternary ammonium)-type Gemini inhibitors reported previously was conducted, as given in Table S1.

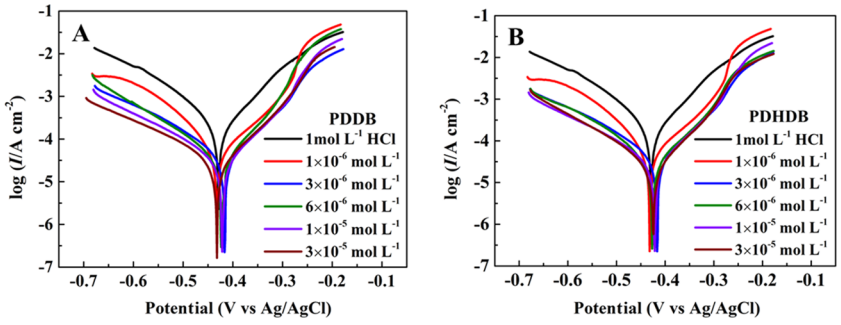

Figure 4. Potentiodynamic polarization curves for carbon steel in 1 mol·L^{-1} HCl without and with different concentrations of PDDB (A) and PDHDB (B).

https://dx.doi.org/10.1021/acsomega.9b02989
ACS Omega 2020, 5, 2620−2629

Table 3. PDP Parameters for Carbon Steel in 1 mol·L^{-1} HCl in the Absence and Presence of Different Concentrations of PDDB and PDHDB

inhibitor	C/mol·L^{-1}	E_{corr}/mV	I_{corr}/mA·cm^{-2}	β_a/V·dec^{-1}	β_c/V·dec^{-1}	η (%)
HCl	0	−429.4	0.2081	0.0889	−0.1226	
PDDB	1×10^{-6}	−430.9	0.0629	0.0908	−0.1265	69.8
	3×10^{-6}	−416.5	0.0413	0.0927	−0.1577	80.2
	6×10^{-6}	−423.4	0.0314	0.0678	−0.1407	84.9
	1×10^{-5}	−422.3	0.0279	0.0719	−0.1671	86.6
	3×10^{-5}	−437.7	0.0235	0.0827	−0.1524	88.7
PDHDB	1×10^{-6}	−431.9	0.0575	0.0865	−0.1186	72.4
	3×10^{-6}	−423.7	0.0361	0.0664	−0.1516	82.7
	6×10^{-6}	−426.9	0.0309	0.0803	−0.1404	85.1
	1×10^{-5}	−431.2	0.0271	0.0825	−0.1331	87.0
	3×10^{-5}	−425.3	0.0233	0.0755	−0.1476	88.8

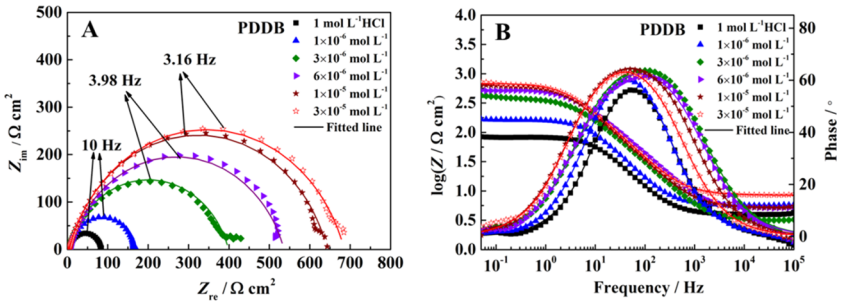

Figure 5. (A) Nyquist plots and (B) Bode and phase angle plots for carbon steel in 1.0 mol·L^{-1} HCl containing different concentrations of PDDB.

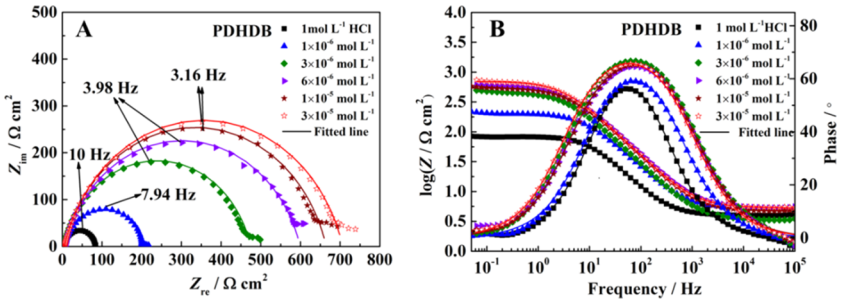

Figure 6. (A) Nyquist plots and (B) Bode and phase angle plots for carbon steel in 1.0 mol·L^{-1} HCl containing different concentrations of PDHDB.

2.5. Electrochemical Impedance Spectroscopy (EIS). EIS measurements can provide the exact and rapid information on the kinetics of electrochemical processes and the surface properties of the investigated systems without destroying the adsorbed layer, thereby allowing one to better understand the corrosion mechanism taking place at the electrode/solution interface. In Figure 5 (for PDDB) and Figure 6 (for PDHDB) are presented Nyquist plots (A) and Bode and phase angle plots (B) for carbon steel in a 1.0 mol·L^{-1} HCl solution without and with different concentrations of inhibitors. From Nyquist plots in Figures 5 and 6, two typical features can be acquired. First, all of the impedance spectra almost present a single capacitive loop with a progressive increment in their diameters with increasing concentrations of PDDB and PDHDB, which implies that the corrosion of carbon steel in 1.0 mol·L^{-1} HCl without and with the addition of two such inhibitors is commonly related to the double-layer behavior and primarily dominated by a charge transfer process. Moreover, a better protective film is formed on the metal surface due to the increasing diameters, accompanied with the incremental inhibitor concentrations.[38,39] Second, all semicircles, illustrated in a complex plane, exhibit a slightly depressed nature, all of the centers of which are located under the abscissa, attributed to the dispersion in the frequency of the interfacial impedance during the corrosion due to the different physical phenomena, such as the surface roughness, impurities, inhomogeneous electrode surface, adsorption of inhibitors, etc.[40] As a result, a frequency-distributed constant phase element (CPE) is, generally, introduced to replace the real double-layer capacitance (C_{dl}) at the metal/solution interface in the equivalent circuit, to accurately determine the impedance parameters and to precisely understand the effects of the roughness and other inhomogeneities.[41]

In all EIS diagrams, Nyquist and Bode plots only exhibited a semicircle capacitive loop and one peak, respectively, indicating the existence of one-time constant (single relaxation process) in all electrochemical processes, which was correlated with the formation of the electrical double layer at the electrode/solution interface.[42] Figure 7 gives a simple one-

https://dx.doi.org/10.1021/acsomega.9b02989
ACS Omega 2020, 5, 2620−2629

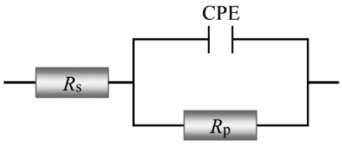

Figure 7. Electrochemical equivalent circuits used to fit the impedance data.

time-constant electrical equivalent circuit, which is employed to analyze the impedance data. In this equivalent circuit, a solution resistance (R_s) is in series connected with a parallel combination of a CPE and a polarization resistance (R_p). Herein, R_p, corresponding to the difference in real impedance at lower and higher frequencies, contains charge transfer resistance R_{ct}, diffuse layer resistance R_d, accumulation resistance R_a and film resistance R_f, i.e., $R_p = R_{ct} + R_d + R_a + R_f$.[43] Figures 5 and 6 also show all fitted results, which are described quite well using this equivalent circuit.

The impedance of CPE (Z_{CPE}) in the equivalent circuit is defined as eq 7[44]

$$Z_{CPE} = Y_0^{-1}(j\omega)^{-n} \quad (7)$$

where Y_0 represents the admittance of the CPE in $s^n \cdot \Omega^{-1} \cdot cm^{-2}$, j is the imaginary unit, ω is the angular frequency in $rad \cdot s^{-1}$, and n is the CPE exponent, as an indicator of the inhomogeneity or roughness of the electrode surface. Herein, the double-layer capacitance, C_{dl}, can be calculated using eq 8[45]

$$C_{dl} = (Y_0 R_p^{1-n})^{1/n} \quad (8)$$

Then, the IE (η) values can be obtained from eq 9[46]

$$\eta = \frac{R_p - R_p^0}{R_p} \times 100\% \quad (9)$$

where R_p^0 and R_p are the polarization resistance values without and with PDDB or PDHDB, respectively. All of the impedance parameters derived from the fitting analyses of EIS profiles are summarized in Table 4.

In the present work, both the R_p and η values exhibit a prominent tendency, i.e., a successive increase with the inhibitor concentration, while the C_{dl} values display an opposite change, i.e., a consecutive decrease. Herein, the R_p values increase from 80.36 $\Omega \cdot cm^2$ (blank) to 681.25 $\Omega \cdot cm^2$ (PDDB) and 702.40 $\Omega \cdot cm^2$ (PDHDB); meanwhile, the maximum η values reach up to 88.2 and 88.6% for PDDB and PDHDB, respectively, at the concentration of 3.0×10^{-5} $mol \cdot L^{-1}$. These results are a likely consequence of the adsorption of more inhibitors on the carbon steel surface as the inhibitor concentration is raised, leading to a higher surface coverage and thus enhancing the inhibition efficiency. In contrast, the reduction in the C_{dl} values is a likely consequence of the increase in the thickness of such adsorbed films and/or the decrease in the local dielectric constant.[29,47,48] Therefore, the variation in R_p, C_{dl}, and η with the PDDB or PDHDB concentrations lends further support to the fact that these inhibitor molecules can fabricate a protective layer via adsorbing on the electrode surface and protect the carbon steel surface from the attack of corrosive media.

One final issue that deserves comment is that the changing trend of η values with the concentrations of PDDB or PDHDB, obtained from the EIS method in Table 4, is also consistent with the results from gravimetric and PDP measurements. In particular, over the entire concentration range studied, PDHDB still exhibits slightly higher IE values than PDDB, especially at low concentrations, implying that the former has a better anticorrosive performance than the latter. This is further confirmed by the quantum chemical calculations. Density functional theory (DFT) results suggest that PDHDB would adsorb on the metal more easily than PDDB and more effectively prevent the metal from corrosion (for more details, see Figure S6 and Table S2).

2.6. Surface Characterization. Scanning electron microscopy (SEM) and the corresponding energy-dispersive spectroscopy (EDS) images for the freshly polished carbon steel coupons in the absence and presence of PDDB or PDHDB are shown in Figure 8. Herein, the EDS images were obtained from the specimens corresponding to the SEM images. The SEM image in Figure 8B gives a rougher surface, derived from the inhibitor-free solution, compared to those in the presence of PDDB (Figure 8C) and PDHDB (Figure 8D) with the inhibited system. This lends direct support to the inhibition action of PDDB and PDHDB in the aggressive media. In Figure 8B, the EDS result of the carbon steel in the uninhibited solution presents the lower characteristic signals of Fe, Mn, and Cu, compared to those of freshly polished or inhibited carbon steel. Herein, Fe peaks are dramatically suppressed and the Fe content is reduced from 96.60% (for freshly polished carbon steel coupon) to 88.57% (for carbon steel in 1.0 $mol \cdot L^{-1}$ HCl solution without any inhibitor). By comparison, the peak corresponding to the O element appears, suggesting the formation of iron oxide in 1.0 $mol \cdot L^{-1}$ HCl solution. These

Table 4. EIS Parameters for Carbon Steel in 1.0 $mol \cdot L^{-1}$ HCl in the Absence and Presence of Different Concentrations of PDDB or PDHDB

inhibitor	$C/mol \cdot L^{-1}$	$R_s/\Omega \cdot cm^2$	$Y_0/\mu S \cdot s^n \cdot cm^{-2}$	n	$C_{dl}/\mu F \cdot cm^{-2}$	$R_p/\Omega \cdot cm^2$	$\chi^2/10^{-4}$	η (%)
HCl	0	3.79 ± 0.21	305.97 ± 9.87	0.8767 ± 0.0123	181.7	80.36 ± 4.46	4.17	
PDDB	1×10^{-6}	5.34 ± 0.50	221.50 ± 4.67	0.8544 ± 0.0068	129.0	169.55 ± 9.40	1.87	52.6
	3×10^{-6}	3.65 ± 0.80	168.60 ± 9.33	0.8272 ± 0.0187	95.5	391.10 ± 6.65	7.88	79.5
	6×10^{-6}	4.41 ± 0.72	131.30 ± 9.37	0.8248 ± 0.0153	74.6	532.70 ± 9.04	9.81	84.9
	1×10^{-5}	4.55 ± 0.74	146.27 ± 2.28	0.8107 ± 0.0123	84.1	637.43 ± 9.50	3.66	87.4
	3×10^{-5}	4.69 ± 0.42	125.20 ± 9.33	0.8241 ± 0.0149	74.0	681.25 ± 0.21	5.89	88.2
PDHDB	1×10^{-6}	4.59 ± 0.93	189.97 ± 9.39	0.8472 ± 0.0077	105.6	202.53 ± 5.88	3.61	60.3
	3×10^{-6}	4.37 ± 0.95	150.30 ± 3.27	0.8351 ± 0.0090	89.1	470.63 ± 7.50	4.66	82.9
	6×10^{-6}	4.98 ± 0.21	118.28 ± 2.92	0.8228 ± 0.0117	66.6	587.40 ± 6.11	4.74	86.3
	1×10^{-5}	4.72 ± 0.74	127.53 ± 9.16	0.8249 ± 0.0153	75.2	653.03 ± 9.01	2.99	87.7
	3×10^{-5}	5.18 ± 0.18	118.00 ± 2.33	0.8212 ± 0.0144	68.6	702.40 ± 1.15	2.98	88.6

https://dx.doi.org/10.1021/acsomega.9b02989
ACS Omega 2020, 5, 2620−2629

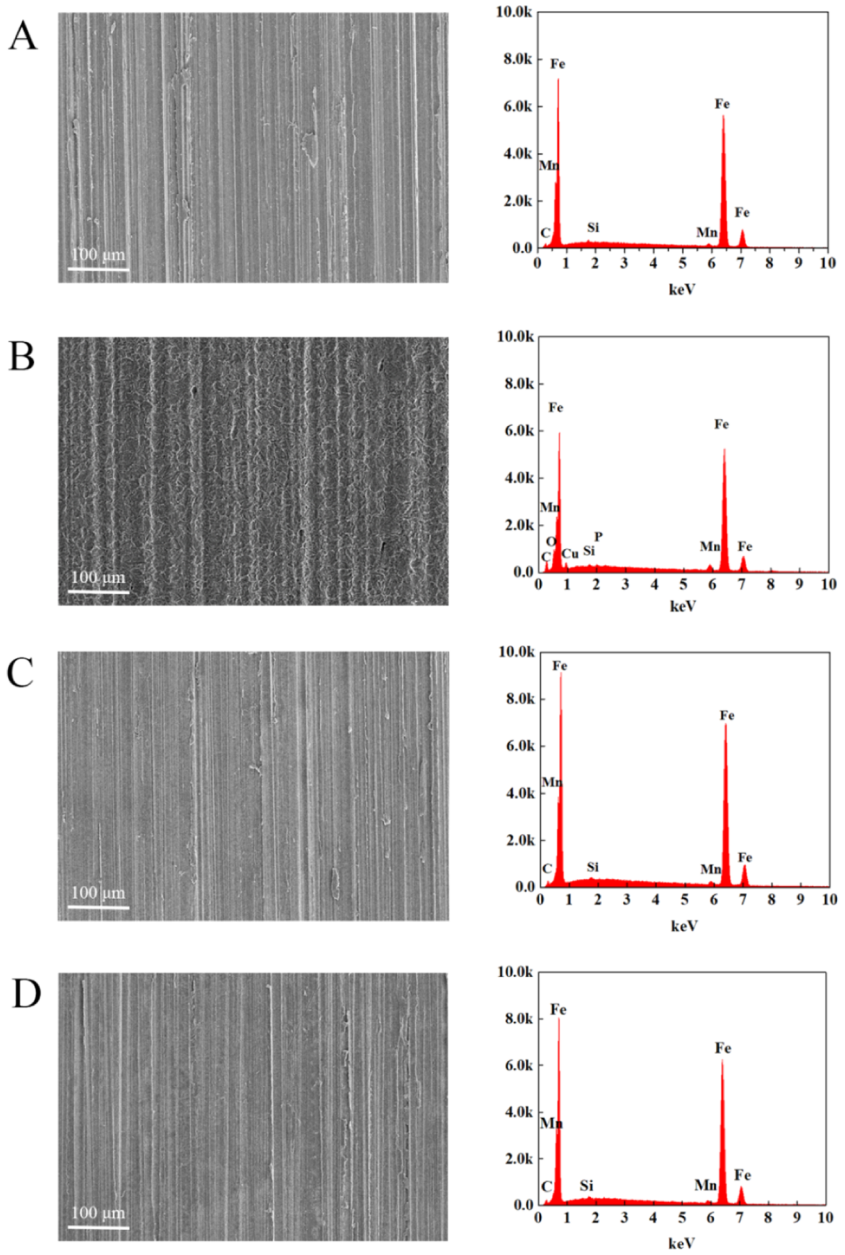

Figure 8. SEM images (left) and the corresponding EDS images (right) obtained from the carbon steel surface after 24 h immersion in 1.0 mol·L^{-1} HCl acid solution: (A) prior to immersion, (B) in the absence of inhibitor, (C) in the presence of 3.0 × 10^{-5} mol·L^{-1} PDDB, and (D) in the presence of 3.0 × 10^{-5} mol·L^{-1} PDHDB.

results indicate that the carbon steel surface is covered with the oxide film in the absence of inhibitors. On the other hand, in the presence of PDDB (Figure 8C) and PDHDB (Figure 8D), the EDS images show an identical result to that of the initial carbon steel. In this work, the mass ratio of Fe almost returns to the initial value, from 88.57% (blank) to 96.54% for PDDB and to 96.48% for PDHDB; meanwhile, the peak of the O element cannot be observed. SEM and EDS results, taken together, indicate that both PDDB and PDHDB can adsorb on the carbon steel surface and significantly retard the corrosion rate of carbon steel so that the chemical composition on the surface almost remains intact.

2.7. Adsorption Mechanism. In this work, the gravimetric, electrochemical, and morphological data, in connection with the isothermal adsorption analysis, illustrate that the addition of PDDB and PDHDB does play a critical role in determining the resultant inhibition performance of the carbon steel in 1.0 mol·L^{-1} HCl solution; moreover, over the entire concentration range studied, PDHDB displays a superior inhibition performance relative to PDDB, which is attributed to the introduction of the hydroxyl groups, allowing the former to have a potential to produce chemisorption to some extent on the carbon steel surface. According to these results, an inhibition mechanism of PDDB and PDHDB is proposed, as shown in Figure 9. In brief, as for PDDB and PDHDB, the dissociated quaternary ammonium bivalent cations can adsorb on the metal surface via the Coulombic attraction with the initially adsorbed anions, like chloride and/or bromide ions; in the case of PDHDB, the electronegative O heteroatom in hydroxyl groups bears lone-pair electrons, which are favorable for the formation of the coordination interactions on the metal surface.

https://dx.doi.org/10.1021/acsomega.9b02989
ACS Omega 2020, 5, 2620−2629

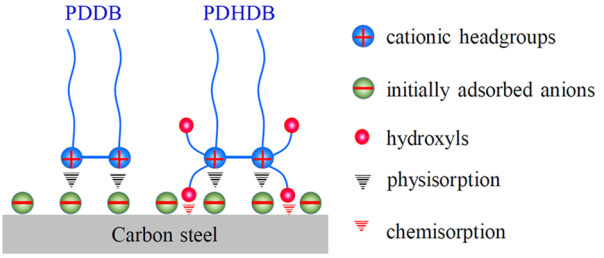

Figure 9. Schematic illustration of the adsorption interactions of PDDB and PDHDB on the carbon steel surface.

3. CONCLUSIONS

In this work, the effect of introducing hydroxyls at the headgroup of cationic Gemini-type inhibitors on the resultant inhibition performance was investigated. Several results are obtained via comparing the inhibitory properties between PDDB and PDHDB.

1. PDDB and PDHDB can serve as an effective corrosion inhibitor, the IEs of which increase with their concentrations.
2. PDDB and PDHDB can act as a mixed-type inhibitor and form a protective layer on the carbon steel surface, resulting in a retarded corrosion rate.
3. PDHDB always displays a better inhibition performance for the carbon steel in 1.0 mol·L^{-1} HCl solution than PDDB, denoting that the introduction of the hydroxyls at the headgroups of such bis(quaternary ammonium) Gemini inhibitors is helpful for enhancing their inhibition action indeed.
4. The adsorption of PDDB and PDHDB conforms to the Langmuir isotherm model, and their ΔG_{ads} values are close to −43.0 kJ·mol^{-1}, indicating that both of them can spontaneously adsorb on the carbon steel surface.

At a more fundamental level, our findings suggest that the modification to the headgroups of Gemini-type inhibitors may be another effective approach to improving their inhibition performance.

4. EXPERIMENTAL SECTION

4.1. Materials and Solution. All chemicals used in this work were of analytical grade and used as received without further purification. The N80 carbon steel applied has the following chemical composition (wt %): 0.35 C, 0.23 Si, 1.46 Mn, 0.011 P, 0.005 S, 0.08 Cu, 0.01 Ni, 0.08 Cr, 0.16 Mo, 0.11 V, 0.024 Al, and balance Fe. All carbon steel coupons, cut from a carbon steel bar, are a three-dimensional cuboid with a length of 5 cm, breadth of 1 cm, and thickness of 0.3 cm, unless specified otherwise.

The simulated corrosion solution of 1.0 mol·L^{-1} hydrochloric acid (HCl) was prepared by diluting an analytically pure concentrated HCl in a mass fraction of 37% with double-distilled water. This solution was also used as a blank sample for comparison. In this work, the concentrations of PDDB and PDHDB ranged from 1.0 × 10^{-6} to 3.0 × 10^{-5} mol·L^{-1}.

4.2. Synthesis of Inhibitors. In this work, the synthesis of PDDB was similar to the procedure reported by Zana et al.,[49] while PDHDB was synthesized using a modified method reported by Wang et al.[50] Their chemical structures were characterized by Fourier transform infrared (FT-IR), ^{1}H, and ^{13}C NMR spectra. The detailed synthesis and spectrum results are given in the Supporting Information.

4.3. Gravimetric Measurements. Gravimetric measurement was carried out using an analytical balance with a precision of ±0.01 mg. Prior to each experiment, the surface of coupons was mechanically abraded with 600, 800, and 1200 grades of emery papers in turn, degreased with acetone, then successively rinsed with ethanol and distilled water, and finally derided in warm air flow. After weighed accurately, three coupons were then immersed in a 1.0 mol·L^{-1} HCl solution of 500 mL in the absence and presence of PDDB or PDHDB at different concentrations for 6 h. The system temperature was controlled at 25.0 ± 0.1 °C using an ultrathermostatic bath. After that, to clean rust products, a chemical method was used, where coupons were immersed in 100 mL of a 1.0 mol·L^{-1} HCl solution containing 0.8 g of hexamethylenetetramine under sonication for about 180 s; rinsed thoroughly with distilled water, acetone, and ethanol in turn; and then dried in warm air flow and weighted accurately again.[51] In this work, average weight losses were obtained from two to three independent measurements for the same sample.

4.4. Electrochemical Measurements. In this work, all electrochemical measurements were conducted using a conventional three-electrode system on a PARSTAT 4000 electrochemical workstation (Princeton Applied Research). Herein, a carbon steel rod, a platinum wire, and a Ag/AgCl (with 3.5 M KCl) electrode were utilized as the working, counter, and reference electrodes, respectively. As working electrodes, a carbon steel rod with a diameter of 1.0 cm was embedded into a poly(tetrafluoroethylene) holder and the void was sealed with epoxy resin so that a flat metal surface with a 0.785 cm^2 surface area was allowed to expose to the aggressive solution. The pretreatment of working electrodes was similar to the procedure used in the gravimetric measurements, in which the end surface of the carbon steel rod was first ground and then degreased, rinsed, and dried finally. Prior to each measurement, the working electrode was immersed in the acid media at the open-circuit potential (OCP) for a fixed time span, 30 min, until a steady state was reached. To check the reproducibility, measurements were independently repeated at least three times for the same specimen. Electrochemical impedance spectroscopy (EIS) spectra were acquired within the frequency range of 100 kHz to 50 mHz, where a sine wave with a 10 mV peak-to-peak amplitude was employed to perturb the testing system. In this work, the corresponding EIS data were carefully fitted and processed with ZSimpWin software. Potentiodynamic polarization (PDP) curves were recorded via varying the potential automatically from −250 to +250 mV versus the OCP at a scan rate of 0.25 mV·s^{-1}. For electrochemical measurements, the cell temperature was also controlled at a constant value of 25.0 ± 0.1 °C using with an ultrathermostatic bath.

4.5. Surface Analysis. Scanning electron microscopy (SEM) and energy-dispersive spectrometry (EDS) were used to assay the surface morphologies and the composition as well. For the surface characterization, the coupons with a size of 1 cm × 1 cm × 0.15 cm were cut from parent plates. After 24 h of immersion in a 1.0 mol·L^{-1} HCl solution without and with 3.0 × 10^{-5} mol·L^{-1} PDDB or PDHDB, the coupons were rinsed using distilled water and ethanol in turn, dried, and then immediately subjected to SEM/EDS analysis.

4.6. Quantum Chemical Calculations. Quantum chemical calculations were performed on PDDB and PDHDB using

https://dx.doi.org/10.1021/acsomega.9b02989
ACS Omega 2020, 5, 2620−2629

Gaussian 09 program package. Herein, the Becke three-parameter hybrid functional together with the Lee−Yang−Parr correlation functional (B3LYP) with 6-31G(d,p) basis set was used to geometrically optimize the molecular structures by density functional theory (DFT).

■ ASSOCIATED CONTENT

Supporting Information

The Supporting Information is available free of charge at https://pubs.acs.org/doi/10.1021/acsomega.9b02989.

Synthesis routes and quantum chemical calculations for compounds PDDB and PDHDB; FT-IR spectra for PDDB and PDHDB (Figure S1); ^{1}H NMR and ^{13}C NMR spectra for PDDB and PDHDB (Figures S2−S5); optimized geometric structures, HOMO and LUMO for compounds PDDB and PDHDB (Figure S6); comparison information between various cationic surfactants as corrosion inhibitors (Table S1); and quantum calculating data for compounds PDDB and PDHDB (Table S2) (PDF)

■ AUTHOR INFORMATION

Corresponding Authors

Chengxian Yin − *State Key Laboratory for Performance and Structure Safety of Petroleum Tubular Goods and Equipment Materials, Tubular Goods Research Institute of China National Petroleum Corporation, Xi'an 710077, China*; Email: yincx@cnpc.com.cn

Qibin Chen − *State Key Laboratory of Chemical Engineering and School of Chemistry & Molecular Engineering, East China University of Science and Technology, Shanghai 200237, China*; orcid.org/0000-0002-1095-1307; Email: qibinchen@ecust.edu.cn

Authors

Minjian Kong − *State Key Laboratory of Chemical Engineering and School of Chemistry & Molecular Engineering, East China University of Science and Technology, Shanghai 200237, China*

Juantao Zhang − *State Key Laboratory for Performance and Structure Safety of Petroleum Tubular Goods and Equipment Materials, Tubular Goods Research Institute of China National Petroleum Corporation, Xi'an 710077, China*

Yuan Wang − *State Key Laboratory for Performance and Structure Safety of Petroleum Tubular Goods and Equipment Materials, Tubular Goods Research Institute of China National Petroleum Corporation, Xi'an 710077, China*

Qingwei Ma − *State Key Laboratory for Performance and Structure Safety of Petroleum Tubular Goods and Equipment Materials, Tubular Goods Research Institute of China National Petroleum Corporation, Xi'an 710077, China*

Honglai Liu − *State Key Laboratory of Chemical Engineering and School of Chemistry & Molecular Engineering, East China University of Science and Technology, Shanghai 200237, China*; orcid.org/0000-0002-5682-2295

Complete contact information is available at: https://pubs.acs.org/10.1021/acsomega.9b02989

Notes

The authors declare no competing financial interest.

■ ACKNOWLEDGMENTS

This work was funded by Open Foundation of The State Key Laboratory for Performance and Structure Safety of Petroleum Tubular Goods and Equipment Materials (2017-FW-76), the National Natural Science Foundation of China (Nos. 21576079, 91834301), the 111 Project of Ministry of Education of China (No. B08021), and the Fundamental Research Funds for the Central Universities of China.

■ REFERENCES

(1) Wang, X.; Yang, H.; Wang, F. Inhibition performance of a gemini surfactant and its co-adsorption effect with halides on mild steel in 0.25 M H_2SO_4 solution. *Corros. Sci.* **2012**, *55*, 145−152.

(2) El-Lateef, H. M. A.; Abo-Riyab, M. A.; Tantawy, A. H. Empirical and quantum chemical studies on the corrosion inhibitionperformance of some novel synthesized cationic gemini surfactantson carbon steel pipelines in acid pickling processes. *Corros. Sci.* **2016**, *108*, 94−110.

(3) Salarvand, Z.; Amirnasr, M.; Talebian, M.; Raeissi, K.; Meghdadi, S. Enhanced corrosion resistance of mild steel in 1 M HCl solution bytrace amount of 2-phenyl-benzothiazole derivatives: Experimental,-quantum chemical calculations and molecular dynamics (MD) simulation studies. *Corros. Sci.* **2017**, *114*, 133−145.

(4) Heakal, F. E. T.; Elkholy, A. E. Gemini surfactants as corrosion inhibitors for carbon steel. *J. Mol. Liq.* **2017**, *230*, 395−407.

(5) Zana, R. Dimeric and oligomeric surfactants. Behavior at interfaces and in aqueous solution: a review. *Adv. Colloid Interface Sci.* **2002**, *97*, 205−253.

(6) Okafor, P. C.; Zheng, Y. G. Synergistic inhibition behaviour of methylbenzyl quaternary imidazoline derivative and iodide ions on mild steel in H_2SO_4 solutions. *Corros. Sci.* **2009**, *51*, 850−859.

(7) Heakal, F. E. T.; Rizk, S. A.; Elkholy, A. E. Characterization of newly synthesized pyrimidine derivatives for corrosion inhibition as inferred from computational chemical analysis. *J. Mol. Struct.* **2018**, *1152*, 328−336.

(8) Hegazy, M. A. A novel Schiff base-based cationic gemini surfactants: Synthesis and effect on corrosion inhibition of carbon steel in hydrochloric acid solution. *Corros. Sci.* **2009**, *51*, 2610−2618.

(9) El-Lateef, H. M. A.; Soliman, K. A.; Tantawy, A. H. Novel synthesized Schiff Base-based cationic gemini surfactants: Electrochemical investigation, theoretical modeling and applicability as biodegradable inhibitors for mild steel against acidic corrosion. *J. Mol. Liq.* **2017**, *232*, 478−498.

(10) Kaczerewska, O.; Leiva-Garcia, R.; Akid, R.; Brycki, B.; Kowalczyk, I.; Pospieszny, T. Effectiveness of O-bridged cationic gemini surfactants as corrosion inhibitors for stainless steel in 3 M HCl: Experimental and theoretical studies. *J. Mol. Liq.* **2018**, *249*, 1113−1124.

(11) Kaczerewska, O.; Leiva-Garcia, R.; Akid, R.; Brycki, B. Efficiency of cationic gemini surfactants with 3-azamethylpentamethylene spacer as corrosion inhibitors for stainless steel in hydrochloric acid. *J. Mol. Liq.* **2017**, *247*, 6−13.

(12) Mobin, M.; Aslam, R.; Aslam, J. Non toxic biodegradable cationic gemini surfactants as novel corrosion inhibitor for mild steel in hydrochloric acid medium and synergistic effect of sodium salicylate: Experimental and theoretical approach. *Mater. Chem. Phys.* **2017**, *191*, 151−167.

(13) Pakiet, M.; Kowalczyk, I. H.; Garcia, R. L.; Akid, R.; Brycki, B. E. Influence of different counterions on gemini surfactants with polyamine platform as corrosion inhibitors for stainless steel AISI 304 in 3 M HCl. *J. Mol. Liq.* **2018**, *268*, 824−831.

(14) Qiu, L. G.; Xie, A. J.; Shen, Y. H. A novel triazole-based cationic gemini surfactant: synthesis and effect on corrosion inhibition of carbon steel in hydrochloric acid. *Mater. Chem. Phys.* **2005**, *91*, 269−273.

(15) Feng, L. W.; Yin, C. X.; Zhang, H. L.; Li, Y. F.; Song, X. H.; Chen, Q. B.; Liu, H. L. Cationic Gemini surfactants with a Bipyridyl

Spacer as corrosion inhibitors for mild steel. *ACS Omega* **2018**, *3*, 18990−18999.
(16) Solmaz, R.; Kardaş, G.; Yazıcı, B.; Erbil, M. Adsorption and corrosion inhibitive properties of 2-amino-5-mercapto-1,3,4-thiadiazole on mild steel in hydrochloric acid media. *Colloids Surf., A* **2008**, *312*, 7−17.
(17) Li, X. H.; Deng, S. D.; Fu, H. Triazolyl blue tetrazolium bromide as a novel corrosion inhibitor for steel in HCl and H_2SO_4 solutions. *Corros. Sci.* **2011**, *53*, 302−309.
(18) Verma, C.; Olasunkanmi, L. O.; Quadri, T. W.; Sherif, E. M.; Ebenso, E. E. Gravimetric, Electrochemical, Surface Morphology, DFT, and Monte Carlo Simulation Studies on Three N-Substituted 2-Aminopyridine Derivatives as Corrosion Inhibitors of Mild Steel in Acidic Medium. *J. Phys. Chem. C.* **2018**, *122*, 11870−11882.
(19) Goulart, C. M.; Esteves-Souza, A.; Martinez-Huitle, C. A.; Rodrigues, C. J. F.; Maciel, M. A. M.; Echevarria, A. Experimental and theoretical evaluation of semicarbazones and thiosemicarbazones as organic corrosion inhibitors. *Corros. Sci.* **2013**, *67*, 281−291.
(20) Migahed, M. A.; Shaban, M. M.; Fadda, A. A.; Alia, T. A.; Negma, N. A. Synthesis of some quaternary ammonium gemini surfactants and evaluation of their performance as corrosion inhibitors for carbon steel in oil well formation water containing sulfide ions. *RSC Adv.* **2015**, *5*, 104480−104492.
(21) Salarvand, Z.; Amirnasr, M.; Talebian, M.; Raeissi, K.; Meghdadi, S. Enhanced corrosion resistance of mild steel in 1 M HCl solution bytrace amount of 2-phenyl-benzothiazole derivatives: Experimental,quantum chemical calculations and molecular dynamics (MD) simulation studies. *Corros. Sci.* **2017**, *114*, 133−145.
(22) Zhang, Q.; Gao, Z. N.; Xu, F.; Zou, X. Adsorption and corrosion inhibitive properties of gemini surfactants in the series of hexanediyl-1,6-bis-(diethyl alkyl ammonium bromide) on aluminium in hydrochloric acid solution. *Colloids Surf., A* **2011**, *380*, 191−200.
(23) Singh, P.; Ebenso, E. E.; Olasunkanmi, L. O.; Obot, I. B.; Quraishi, M. A. Electrochemical, Theoretical, and Surface Morphological Studies of Corrosion Inhibition Effect of Green Naphthyridine Derivatives on Mild Steel in Hydrochloric Acid. *J. Phys. Chem. C* **2016**, *120*, 3408−3419.
(24) Obot, I. B.; Obi-Egbedi, N. O.; Umoren, S. A. Antifungal drugs as corrosion inhibitors for aluminium in 0.1M HCl. *Corros. Sic.* **2009**, *51*, 1868−1875.
(25) Morad, M. S.; Sarhan, A. A. O. Application of some ferrocene derivatives in the field of corrosion inhibition. *Corros. Sci.* **2008**, *50*, 744−753.
(26) Deng, S.; Li, X.; Fu, H. Acid violet 6B as a novel corrosion inhibitor for cold rolled steel in hydrochloric acid solution. *Corros. Sci.* **2011**, *53*, 760−768.
(27) Hegazy, M. A.; Zaky, M. F. Inhibition effect of novel nonionic surfactants on the corrosion of carbon steel in acidic medium. *Corros. Sci.* **2010**, *52*, 1333−1341.
(28) Liu, Y.; Zou, C. J.; Yan, X. L.; Xiao, R. J.; Wang, T. Y.; Li, M. *β*-Cyclodextrin Modified Natural Chitosan as a Green Inhibitor for Carbon Steel in Acid Solutions. *Ind. Eng. Chem. Res.* **2015**, *54*, 5664−5672.
(29) Mobin, M.; Aslam, R.; Aslam, J. Synergistic effect of cationic gemini surfactants and butanol on the corrosion inhibition performance of mild steel in acid solution. *Mater. Chem. Phys.* **2019**, *223*, 623−633.
(30) Ahamad, I.; Prasad, R.; Quraishi, M. A. Inhibition of mild steel corrosion in acid solution by Pheniramine drug: Experimental and theoretical study. *Corros. Sci.* **2010**, *52*, 3033−3041.
(31) Solmaz, R. Investigation of adsorption and corrosion inhibition of mild steel in hydrochloric acid solution by 5-(4-Dimethylaminobenzylidene)rhodamine. *Corros. Sci.* **2014**, *79*, 169−176.
(32) Deng, S.; Li, X.; Fu, H. Two pyrazine derivatives as inhibitors of the cold rolled steel corrosion in hydrochloric acid solution. *Corros. Sci.* **2011**, *53*, 822−828.
(33) Amin, M. A.; Ahmed, M. A.; Arida, H. A.; Kandemirli, F.; Saracoglu, M.; Arslan, T.; Basaran, M. A. Monitoring corrosion and corrosion control of iron in HCl by nonionic surfactants of the TRITON-X series-Part III. Immersion time effects and theoretical studies. *Corros. Sci.* **2011**, *53*, 1895−1909.
(34) Saleh, M. M.; Mahmoud, M. G.; Abd El-Lateef, H. M. Comparative study of synergistic inhibition of mild steel and pure iron by 1-hexadecylpyridinium chloride and bromide ions. *Corros. Sci.* **2019**, *154*, 70−79.
(35) Cao, C. On electrochemical techniques for interface inhibitor research. *Corros. Sci.* **1996**, *38*, 2073−2082.
(36) Popova, A.; Christov, M.; Vasilev, A. Inhibitive properties of quaternary ammonium bromides of N-containing heterocycles on acid mild steel corrosion. Part I: Gravimetric and voltammetric results. *Corros. Sci.* **2007**, *49*, 3276−3289.
(37) Odewunmi, N. A.; Umoren, S. A.; Gasem, Z. M. Watermelonwaste products as green corrosion inhibitors for mild steel in HCl solution. *J. Environ. Chem. Eng.* **2015**, *3*, 286−296.
(38) Aslam, R.; Mobin, M.; Zehra, S.; Obot, I. B.; Ebenso, E. E. N,N′-Dialkylcystine Gemini and Monomeric N-Alkyl Cysteine Surfactants as Corrosion Inhibitors on Mild Steel Corrosion in 1 M HCl Solution: A Comparative Study. *ACS Omega* **2017**, *2*, 5691−5707.
(39) Yohai, L.; Vázquez, M.; Valcarce, M. B. Phosphate ions as corrosion inhibitors for reinforcement steel in chloride-rich environments. *Electrochim. Acta* **2013**, *102*, 88−96.
(40) El-Lateef, H. M. A.; Ahmed, H. T. Synthesis and evaluation of novel series of Schiff base cationic surfactants as corrosion inhibitors for carbon steel in acidic/chloride media: experimental and theoretical investigations. *RSC Adv.* **2016**, *6*, 8681−8700.
(41) Popova, A.; Christov, M.; Vasilev, A. Inhibitive properties of quaternary ammonium bromides of N-containing heterocycles on acid mild steel corrosion. Part II: EIS results. *Corros. Sci.* **2007**, *49*, 3290−3302.
(42) Motamedi, M.; Tehrani-Bagha, A. R.; Mahdavian, M. Effect of aging time on corrosion inhibition of cationic surfactant on mild steel in sulfamic acid cleaning solution. *Corros. Sci.* **2013**, *70*, 46−54.
(43) Solmaz, R.; Kardaş, G.; Çulha, M.; Yazıcı, B.; Erbil, M. Investigation of adsorption and inhibitive effect of 2-mercaptothiazoline on corrosion of mild steel in hydrochloric acid media. *Electrochim. Acta* **2008**, *53*, 5941−5952.
(44) Olasunkanmi, L. O.; Obot, I. B.; Kabanda, M. M.; Ebenso, E. E. Some Quinoxalin-6-yl Derivatives as Corrosion Inhibitors for Mild Steel in Hydrochloric Acid: Experimental and Theoretical Studies. *J. Phys. Chem. C* **2015**, *119*, 16004−16019.
(45) Lebrini, M.; Robert, F.; Vezin, H.; Roos, C. Electrochemical and quantum chemical studies of some indole derivatives as corrosion inhibitors for C38 steel in molar hydrochloric acid. *Corros. Sci.* **2010**, *52*, 3367−3376.
(46) Döner, A.; Kardaş, G. N-Aminorhodanine as an effective corrosion inhibitor for mild steel in 0.5 M H_2SO_4. *Corros. Sci.* **2011**, *53*, 4223−4232.
(47) Ghanbari, A.; Attar, M. M.; Mahdavian, M. Corrosion inhibition performance of three imidazole derivatives on mild steel in 1 M phosphoric acid. *Mater. Chem. Phys.* **2010**, *124*, 1205−1209.
(48) Ehsani, A.; Mahjani, M. G.; Moshrefi, R.; Mostaanzadeha, H.; Shayehb, J. S. Electrochemical and DFT Study on the Inhibition of 316L Stainless Steel Corrosion in Acidic Medium by 1-(4-nitrophenyl)-5-amino-1H-tetrazole. *RSC Adv.* **2014**, *4*, 20031−20037.
(49) Zana, R.; Benrraou, M.; Rueff, R. Alkanediyl-*α*,*ω*-*bis*(dimethylalkylammonium bromide) surfactants. 1. Effect of the spacer chain length on the critical micelle concentration and micelle ionization degree. *Langmuir* **1991**, *7*, 1072−1075.
(50) Huang, X.; Han, Y. C.; Wang, Y. X.; Cao, M. W.; Wang, Y. L. Aggregation properties of cationic gemini surfactants with dihydroxyethylamino headgroups in aqueous solution. *Colloids Surf., A* **2008**, *325*, 26−32.
(51) Hegazy, M. A.; Badawi, A. M.; Abd El Rehim, S. S.; Kamel, W. M. Corrosion inhibition of carbon steel using novel N-(2-(2-mercaptoacetoxy)ethyl)-N,N-dimethyl dodecan-1-aminium bromide during acid pickling. *Corros. Sci.* **2013**, *69*, 110−122.

https://dx.doi.org/10.1021/acsomega.9b02989
ACS Omega 2020, 5, 2620−2629